ISSN 1674-1056
http://cpb.iphy.ac.cn
http://iopscience.iop.org/cpb
中国物理 B
Chinese Physics
中国物理 Chinese Physics B

Structural, electronic, and mechanical properties of cubic TiO_2:A first-principles study

Debashish Dash, Chandan K Pandey, Saurabh Chaudhury, Susanta K Tripathy
Citation: Chin. Phys. B . 2018, 27(1): 017102. **doi:** 10.1088/1674-1056/27/1/017102

Journal homepage: http://cpb.iphy.ac.cn; http://iopscience.iop.org/cpb

What follows is a list of articles you may be interested in

Tuning electronic properties of the S_2/graphene heterojunction by strains from density functional theory

Jun-Hui Lei(雷军辉), Xiu-Fen Wang(王秀峰), Jian-Guo Lin(林建国)
Chin. Phys. B . 2017, 26(12): 127101. **doi:** 10.1088/1674-1056/26/12/127101

Strain engineering of electronic and magnetic properties of Ga_2S_2 nanoribbons

Bao-Ji Wang(王宝基), Xiao-Hua Li(李晓华), Li-Wei Zhang(张利伟), Guo-Dong Wang(王国东), San-Huang Ke(柯三黄)
Chin. Phys. B . 2017, 26(5): 057102. **doi:** 10.1088/1674-1056/26/5/057102

New ternary superconducting compound $LaRu_2As_2$: Physical properties from density functional theory calculations

M A Hadi, M S Ali, S H Naqib, A K M A Islam
Chin. Phys. B . 2017, 26(3): 037103. **doi:** 10.1088/1674-1056/26/3/037103

Stability, electronic structures, and mechanical properties of Fe-Mn-Al system from first-principles calculations

Ya-Hui Liu(刘亚会), Xiao-Yu Chong(种晓宇), Ye-Hua Jiang(蒋业华), Jing Feng(冯晶)
Chin. Phys. B . 2017, 26(3): 037102. **doi:** 10.1088/1674-1056/26/3/037102

Electronic structure of O-doped SiGe calculated by DFT+*U* method

Zong-Yan Zhao(赵宗彦), Wen Yang(杨雯), Pei-Zhi Yang(杨培志)
Chin. Phys. B . 2016, 25(12): 127101. **doi:** 10.1088/1674-1056/25/12/127101

Structural, electronic, and mechanical properties of cubic TiO_2: A first-principles study

Debashish Dash[1,†], Chandan K Pandey[1], Saurabh Chaudhury[1], and Susanta K Tripathy[2]

[1] *Department of Electrical Engineering, National Institute of Technology, Silchar, Assam* 788010, *India*
[2] *Department of Electronics and Communication Engineering, National Institute of Technology, Silchar, Assam* 788010, *India*

(Received 1 August 2017; revised manuscript received 29 September 2017; published online 17 November 2017)

We present an analysis of structural, electronic, and mechanical properties of cubic titanium dioxide (TiO_2) using an all electron orthogonalzed linear combinations of atomic orbitals (OLCAO) basis set under the framework of density functional theory (DFT). The structural property, especially the lattice constant *a*, and the electronic properties such as the band diagram and density of states (DOS) are studied and analyzed. The mechanical properties such as bulk moduli, shear moduli, Young's Moduli, and Poison's ratio are also investigated thoroughly. The calculations are carried out on shear moduli and anisotropy factor for cubic TiO_2. The Vickers hardness is also tested for fluorite and pyrite cubic-structured TiO_2. Furthermore, the results are compared with the previous theoretical and experimental results. It is found that DFT-based simulation produces results which are approximation to experimental results, whereas the calculated elastic constants are better than the previous theoretical and experimental values.

Keywords: density functional theory, cubic TiO_2, structural, electronic, and mechanical properties

PACS: 71.15.Mb, 77.84.Bw **DOI:** 10.1088/1674-1056/27/1/017102

1. Introduction

TiO_2 is found in nature in many different structures and crystalline forms such as monoclinic, orthorhombic, simple tetragonal, and cubic.[1] It provides many different utilizations when it is grown in different polymorphic forms. In nature, titanium dioxide forms in three different ways, namely, rutile, anatase, and brookite.[2] Since the last decade, different types of advanced materials have been invented by applying high pressure on the crystal structure for various electronic applications. Yugui *et al.* synthesized platinum nitride as a noble nitride material under high pressure and high temperature in its crystalline form.[3] They found out the electronic properties using Raman scattering and the mechanical properties like bulk modulus and shear modulus using Voight, Reuss, and Hill (VRH) theory. Similarly, Wuming *et al.* described different mechanical properties of the earth and analyzed how the high pressure variations change the earth's mantle.[4] Li *et al.* used laser light excitation to investigate the Raman and photoluminescence spectra of Y_2O_3/Eu^{3+} and $Y_2O_3/Eu^{3+}/Mg^{2+}$ nanorods under high pressure and noticed that a structural transition from cubic to amorphous takes place when the pressure increases above 24 GPa.[5] They also found that when the pressure is 8 GPa, distorted phases of Raman and photoluminescence spectra become visible.[5] Moreover, Wang *et al.* investigated disordered materials using the synchrotron radiation-based technique and the pressure-induced phase transformation of disordered alloys. They reported the mechanical behavior and how Shanghai synchrotron radiation facility (SSRF) helps to investigate various structural properties of different disordered materials.[6,7] Thus, it is clear that high pressure plays as an important role of catalyst in converting a material from one form to another for different applications. In the last decade, titanium dioxide has been extensively studied both theoretically and experimentally due to its numerous advantages like non-toxicity, low cost, long-term stability and also due to its superb catalytic feature.[8] By applying high pressures, titania is grown in many different forms such as orthorhombic, columbite, cotunnite, monoclinic baddeleyite, and cubical.[9] When a high pressure is applied to rutile/anatase type polymorphs (eg., SnO_2, PbO_2, HfO_2, and RuO_2), they get converted to the isostructural type of fluorite (CaF_2) or pyrite (FeS_2) structure. Investigations are still in the infant stage to explore different applications of titanium dioxide polymorphs. Some distinguished industrial and commercial applications of TiO_2 such as self-cleaning tiles, self-cleaning paints, windows panes, transparent windows and glasses, high efficiency solar cells, dynamic random access modules, and creating super hard materials are highly encouraged in the present era.[10] However, considering future conservation of energy and cleanliness of environment, the solar cell is the most important application for which cubic TiO_2 is highly preferred.[11] In general, the cubic TiO_2 is synthesized from anatase TiO_2 by heating at a high temperature of 1900–2100 K in a diamond-anvil cell under a pressure of 48 GPa.[12–14] Investigations on both phases of cubic TiO_2 have been carried out by many researchers both experimentally and

†Corresponding author. E-mail: debashishdashnits@gmail.com

© 2018 Chinese Physical Society and IOP Publishing Ltd

theoretically. Initially, Swamy and Muddle[15] concluded that the theoretical values of pyrite TiO_2 are closer to the experimental values, except a lower bulk modulus. However, Liang *et al.*[13] found little difference between both the phases of cubic TiO_2, which contradicts the facts given by Swamy and Muddle.[15] According to Mattesini *et al.*,[16,17] the only difference between the two cubic phases of TiO_2 is the positions of oxygen atoms located. In pyrite TiO_2, the oxygen atoms are located at $\pm(0.34, 0.34, 0.34)$; whereas in fluorite structure, these are at $\pm(0.25, 0.25, 0.25)$. Later on, Kim *et al.*[18] performed a number of experiments and concluded that pyrite TiO_2 is unstable because of the imaginary frequencies in the phonon spectra during the entire pressure range, however fluorite TiO_2 is stable because of the absence of such imaginary frequencies. Miloua *et al.*[8] studied both cubical TiO_2 in detail using the full potential linearized augmented plane wave method. Similarly, Zhao *et al.* investigated various material parameters such as diffusion and interfacial energy using atomic simulations.[19] In the same way, Hu *et al.* carried out a deep study on the electronic and other properties using density functional theory (DFT) and other ultra-soft pseudopotentials.[20]

From the literature, it is clear that numerous investigations have been carried out for natural TiO_2. Additionally, a few investigations on the structural, electronic, and elastic properties for a catalytic material are also available. However, exploration of material properties under high pressure is quite neglected. Detailed investigations on cubic TiO_2 in a systematic way are rare due to ambiguity of experimental and simulated results. Hence, detailed investigations of structural, electronic, and elastic properties of cubic TiO_2 under high pressure are motivated for different applications. In this paper, a systematic *ab-initio* investigation of the structural, electronic, and mechanical properties of cubic TiO_2 under high pressure is carried out using the orthogonalized linear combinations of atomic orbitals (OLCAO) method. The rest of the paper is organized as follows. Section 2 describes various computational methods adopted in this study of TiO_2. The results and discussion are present in Section 3. Finally, conclusions are drawn in Section 4.

2. Computational methods

In this paper, computations are carried out only for fluorite and pyrite type TiO_2. Fluorite is known as the conventional cubic cell, having a space group of $Fm\bar{3}m(225)$, whereas pyrite TiO_2 is known to be isostructural to the modified fluorite structure, having a space group of $pa\bar{3}(205)$.[21] The lattice parameters considered here are $a = b = c =$ 4.787 Å for fluorite and $a = b = c = 4.844$ Å for pyrite TiO_2, and the structure has been optimized using maximized force. Zero constraints are assumed for optimization and the limited memory Broyden–Fletcher–Goldfarb–Shanno (LBFGS) algorithm[22–25] is utilized as the optimization method because of its popularity for parameter estimation in machine learning. The BFGS algorithm is a quasi-Newton method, which converges as early as possible compared to other algorithms like the conjugate gradient (CG) optimization technique. The LBFGS algorithm works on the approximate Hessian matrix. In each iteration, it updates the approximated Hessian matrix by using vector–vector products. With fewer iterations, it reaches into its local minimum without sticking at the time of calculation. But for intermediate calculations, it needs a huge amount of memory for storing the temporary approximated Hessian matrix; and if more intermediate results are stored, then there is a chance of losing convergence. To avoid this problem, it is preferable to use the limited memory BFGS. Furthermore, energy minimization by varying lattice constants is also carried out. During the simulation, the default lattice parameters of both crystals are varied within ±15% and then we obtain the characteristic curves between the total energy in Hartree and the total volume in $Bohr^3$, which are shown in Figs. 1(a) and 1(b) for fluorite and pyrite TiO_2, respectively. The lowest energy lattice constants are considered for simulation because minimizing the total energy of the crystal determines an appropriate set of linear combination of

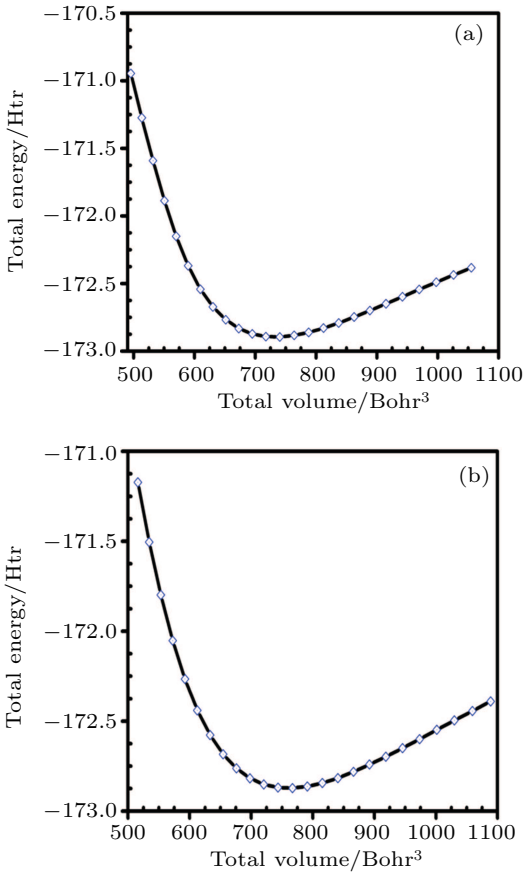


Fig. 1. (color online) Total energy vs. total volume for (a) fluorite-structured TiO_2 and (b) pyrite-structured TiO_2.

coefficients. For simulation, the orthogonalized linear combinations of atomic orbitals method[26] is adopted here, which is an all-electron technique adopted for calculating $3p^6 4s^2 3d^2$ and $2s^2 2p^4$ states as valence electrons for Ti and O, respectively. The optimized lattice structures of fluorite and pyrite TiO_2 are shown in Figs. 3(a) and 3(b), respectively. This method correctly predicts the molecular orbitals due to the orthogonal simulation pattern. The LCAO method initially assumes that the total number of molecular orbitals is equal to the total number of atomic orbitals included in the linear expansion. In other words, n atomic orbitals combine to form n molecular orbitals. The OLCAO is implemented in the framework of density functional theory having the exchange correlation type of local density approximation (LDA). For the simulation of various parameters, Dirac–Bloch exchange with Perdew–Zunger (PZ) correlation[27] is considered. Other parameters like Hubbard U, spin–orbit coupling, and van der Waals corrections are disabled. The grid mesh cut-off is taken as 1633 eV (60 Hartree). The Monkhorst–Pack scheme[28] is used for the k-point sampling, which is $12 \times 12 \times 12$ for fluorite TiO_2 with a total of 864 symmetric points in the first Brillouin zone and $4 \times 4 \times 4$ for pyrite TiO_2 with 32 symmetric points in the first Brillouin zone.[29] Double zeta polarized basis sets are used for calculation. For the oxygen atoms, the Fritz-Haber-Institute (FHI) [$Z = 6$] LDA PZ pseudopotential has been used, whereas for the titanium atoms, the FHI [$Z = 4$] LDA PZ pseudopotential has been used.

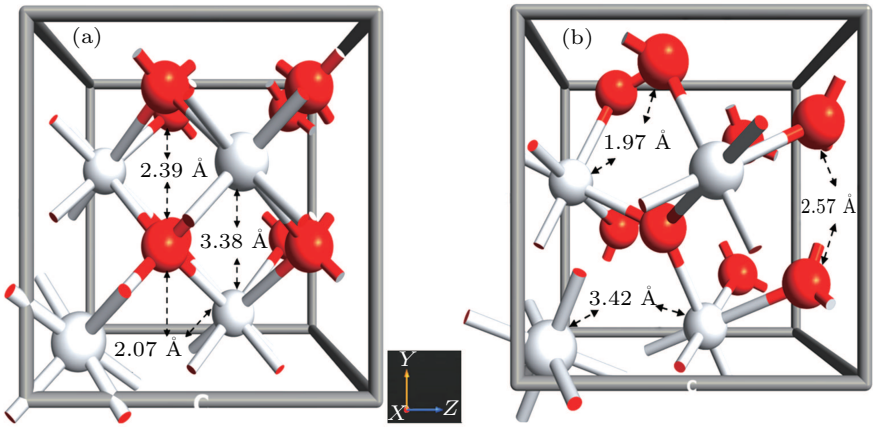


Fig. 2. (color online) (a) Optimized fluorite TiO_2 with distance between Ti's, O's, and Ti–O atoms. (b) Optimized pyrite TiO_2 with distance between Ti's, O's, and Ti–O atoms. White balls represent Ti atoms and red balls represent O atoms.

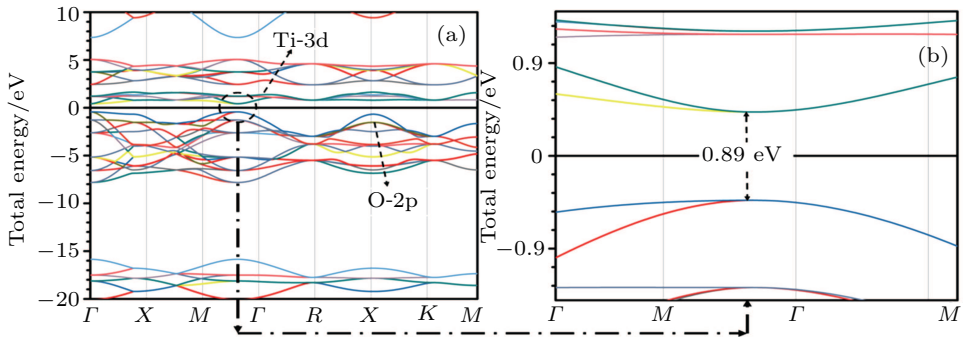


Fig. 3. (color online) (a) Band diagram for fluorite TiO_2 and (b) energy band gap between VBM and CBM.

3. Results and discussion

With the framework presented in the previous section, the simulation results and analysis on the structural, electronic, and mechanical properties of fluorite and pyrite TiO_2 are presented in this section in detail. The simulations are carried out in a HP workstation with 12 GB RAM (Z380) using Virtual Nano Lab software from Quantumwise Atomistix Tool Kit (ATK).[30–32]

3.1. Structural properties

First of all, a systematic structured optimization has been carried out for both phases of TiO_2 over a wide range of lattice parameters. As all the physical properties are related with the total energy, so those lattice constants which give a minimum total energy are considered as the equilibrium lattice constants. If the total energy is obtained, then any of the physical properties related to the total energy can be easily calculated.

Both the fluorite and pyrite titanium dioxide structures are cubic in nature and are considered for simulation. The optimized lattice constants for fluorite and pyrite structures

are shown in Fig. 2. The geometrical configuration of the pyrite phase is given with the distance between Ti and O atoms $d_{\mathrm{Ti-O}} = 1.97$ Å, the distance between two O ions $d_{\mathrm{O-O}} = 2.57$ Å, and the distance between two titanium atoms $d_{\mathrm{Ti-Ti}} = 3.42$ Å. Similarly, for the fluorite phase, $d_{\mathrm{Ti-O}} = 2.07$ Å, $d_{\mathrm{O-O}} = 2.39$ Å, and $d_{\mathrm{Ti-Ti}} = 3.38$ Å.

The equilibrium lattice constants, the bulk modulus, and other properties have been simulated using Birch–Murnaghan's equation of state (EOS)[33,34] in LCAO-based calculations. The totally relaxed Wyckoff positions and cell volume are considered during simulation. The results are compared with the theoretical and experimental values reported earlier. The lattice parameter obtained for fluorite-structured TiO_2 is 1.7% smaller compared to the experimental values.[35] Here, for all the calculations, the optimized minimum energy lattice parameters computed earlier are used. The bulk moduli of fluorite and pyrite TiO_2 using OLCAO are found to be 296.2 and 270.83, respectively. The bulk modulus of fluorite TiO_2 is higher (about 3%–4%) compared to the theoretical results given in Refs. [8], [9], [12], and [35]. It can be seen that the calculated value is very close to the other exchange correlation-based values given in Refs. [10] and [13]. This small difference may be due to better optimization algorithm and the use of different density-functional-based electronic structure. Similarly, for the pyrite structure, the calculated bulk modulus is much closer (about 0.7% to 3.17% undervalued) to the other calculated values given in Refs. [9], [12], and [13].

3.2. Elastic properties

Elastic property is directly related to various solid state properties and creates a link between the mechanical and dynamical behaviors of crystals. It also provides information regarding the interatomic potential, phonon spectra, and more importantly the nature of the forces operating in solids. Much information regarding material properties can be obtained from the elasticity matrix. Generally, it provides the bonding character between adjacent atomic planes, the bonding anisotropy, the stability of the structure, and the stiffness of the material. So their *ab-initio* calculation requires precise ways of computation. Basically, the forces and elastic constants are functions of the first-order and the second-order derivatives of the potentials.[36–39]

Here, to compute the independent elastic constants C_{ij}, assumptions of small lattice distortions are made in order to remain within the elastic domain of the crystal. As both crystals are cubic in nature, there are only three independent elastic constants C_{11}, C_{12}, and C_{44}.[9] With the help of these three elastic independent constants, the mechanical stability can be determined. Initially, the positive definiteness of the stiffness matrix should be checked before proceeding to further calculations. The conditions are as follows:[40,41]

$$c_{11} > |c_{12}|, \quad c_{11} > 0, \quad c_{44} > 0,$$

$$(c_{11} + 2c_{12}) > 0. \tag{1}$$

If all the above conditions are satisfied, then the material is mechanically stable.

The bulk modulus (B) and shear modulus (G) are calculated using two different theories, such as Reuss theory and Voigt theory. B_{R} and G_{R} are used here to represent the bulk and the shear moduli obtained using the Reuss theory,[42] whereas B_{V} and G_{V} represents the bulk and the shear moduli obtained using the Voigt theory.[43] Under the Reuss approximation, B_{R} and G_{R} are expressed as

$$B_{\mathrm{R}} = (3s_{11} + 6s_{12})^{-1}, \tag{2}$$

$$G_{\mathrm{R}} = 5\,(4s_{11} - 4s_{12} + 3s_{44})^{-1}, \tag{3}$$

where s_{11}, s_{12}, and s_{44} are the compliance matrix elements of both phases of TiO_2. By using the Voigt theory, B_{V} and G_{V} are expressed as

$$B_{\mathrm{V}} = \frac{(c_{11} + 2c_{12})}{3}, \tag{4}$$

$$G_{\mathrm{V}} = \frac{(C_{11} - C_{12} + 3C_{44})}{5}. \tag{5}$$

Hill[44] suggested that the actual effective elastic moduli of anisotropic crystalline materials should be approximated by the arithmetic mean of bulk and shear moduli. As per the Hill approximation, the bulk modulus B_{Hill} and shear modulus G_{Hill} are given as

$$B_{\mathrm{Hill}} = \frac{(B_{\mathrm{R}} + B_{\mathrm{V}})}{2}, \tag{6}$$

$$G_{\mathrm{Hill}} = \frac{(G_{\mathrm{R}} + G_{\mathrm{V}})}{2}. \tag{7}$$

It is well known that the bulk and shear moduli are measures of hardness of any crystalline solid. The bulk modulus is a measure of resistance to volume change by the applied pressure. The shear modulus is a measure of resistance to reversible deformations upon shear stress. Thus, the shear modulus is a better predictor of hardness than the bulk modulus. Generally, the shear modulus mainly depends on C_{44}. The larger C_{44} is, the larger the shear modulus will be. C_{44} of pyrite TiO_2 is larger because the deformity of oxygen atoms from cubic to rhombohedral largely enhances the rigidity against the shape deformations at some directions. If the shear modulus is larger, the material is harder. Thus, the shear modulus is a measure of resistance to the shape change and is more pertinent to hardness. Here, for the fluorite-structured TiO_2, the bulk modulus is found to be 296.2, whereas the shear modulus is 68.126. For pyrite TiO_2, the bulk modulus is 270.83 but the shear modulus is about 100 which is quite large compared to that of fluorite TiO_2. So pyrite TiO_2 is much harder than fluorite TiO_2. Later, by using Vickers hardness, it is also proved that pyrite TiO_2 is harder than fluorite TiO_2. All the calculated values are listed in Tables 1 and 2.

Table 1. Structural, electronic, and elastic properties of cubic TiO_2 using the OLCAO, single-crystal (SC), Voight–Reuss–Hill (VRH), and Hashing–Shtrikman (HS) schemes and other exchange correlation methods used with LDA.

Phase	Method	a/Å	Vol./Å^3	B_0/GPa	E_g/eV	Ref.
Fluorite ($Fm3m$)	OLCAO-PZ	4.787	109.696	296.2	0.89(D)	This study
	SC-LDA	4.742	106.631	288.7		[8]
	VRH-LDA			292.3		[8]
	HS-LDA			292.3		[8]
	LDA	4.7412	106.577	284.5	1.061(I)	[9]
	LCAO-LDA	4.75	107.04	308		[10]
	VASP-LDA	4.748	107.08	309		[10]
	LDA-CAPZ	4.739	106.429	285	1.065(D)	[12]
	LDA-CASTEP	4.749	107.104	289, 266	1.08(D)	[13]
	BSTATE-LDA	4.728	105.73	324		[13]
	PP-PW-PBE	4.762	107.986		1.042(I)	[14]
	LDA	4.870	115.5		1.79(D), 1.04(I)	[16]
	experiment	4.516	92.1	202		[17]
Pyrite ($Pa\bar{3}$)	OLCAO-PZ	4.844	113.661	270.83	1.18(ID)	This study
	LDA	4.809	111.215	279.7	1.438(ID)	[9]
	LCAO-LDA	4.8	110.66	273		[10]
	VASP-LDA	4.821	112.10	298		[10]
	LDA-CAPZ	4.807	111.1	276.43	1.451(ID)	[12]
	BSTATE-LDA	4.886	116.65	272		[12]
	VASP-LDA	4.821	112.10	298		[12]
	CASTEP-LDA	4.805	110.95	304		[12]
	BSTATE-LDA	4.796	110.36	320		[13]
	LCAO-LDA	4.800	110.66	273		[13]
	LDA	4.813	111.49		1.81(D) 1.44(ID)	[16]

Table 2. Elastic constants C_{ij}, calculated anisotropy A, shear modulus G, Young's modulus Y, Poisson's ratio υ, and Vickers hardness H_v.

Phase	Method	C_{11}	C_{12}	C_{44}	A	G	Y	υ	H_v	Ref.
Fluorite ($Fm3m$)	OLCAO-PZ	523.09	180.66	32.6	0.19	68.126	431.03	0.393	1.23	This study
	LDA	663.3	95.1	31.8	0.11	91.0	246.7	0.355		[9]
	SC-LDA	665.5	105.7	59.4	0.21	280	636.6	0.14		[8]
	LDA	670.3	103.5	68.6	0.24	154.5	394.1	0.275		[8]
	LDA-CAPZ	665	94	37.5	0.13	57	642	0.124		[12]
	BSTATE-LDA	687	143	73	0.19	128	339	0.326		[13]
	VASP-LDA	671	128	40	0.14	97	263	0.358		[13]
	CASTEP-LDA	670	99	53	0.18	112	298	0.328		[13]
Pyrite ($Pa\bar{3}$)	OLCAO-PZ	430.58	190.70	88.39	0.73	99.9	313.47	0.335	5.94	This study
	LDA	459	189.9	100.8	0.74	113.2	299.2	0.322		[9]
	LDA-CAPZ	447	191	95.85	0.74	106.6	333	0.30		[12]
	BSTATE-LDA	545	201	133	0.77	130	344	0.318		[13]
	VASP-LDA	454	198	100	0.78	110	292	0.328		[13]
	CASTEP-LDA	491	199	113	0.77	125	328	0.315		[13]

There is another averaging scheme known as Hashing–Shtrikman (HS). The shear modulus using HS scheme[8,45] is expressed as

$$G_{HS+} = C_{44} + 2\left(\frac{5}{G - C_{44}} + \frac{18\,(B + 2C_{44})}{5C_{44}\,(3B + 4C_{44})}\right), \quad (8)$$

$$G_{HS-} = G + 3\left(\frac{5}{C_{44} - G} + \frac{12\,(B + 2G)}{5G\,(3B + 4G)}\right). \quad (9)$$

By averaging both, the shear modulus in the HS scheme can be given as

$$G_{HS} = \frac{1}{2}\,(G_{HS+} + G_{HS-})\,. \quad (10)$$

Whereas the shear modulus for single crystal is calculated as

$$G_{SC} = \frac{(C_{11} - C_{12})}{2}. \quad (11)$$

By comparing all the shear moduli, it is observed that $G_{VRH} < G_{HS} < G_{SC}$ for both structures of cubic TiO_2.

Young's modulus can be defined as the ratio of stress and strain, which basically is used to measure the stiffness of the solid. If the Young's modulus is high, then the material is stiffer. The Young's modulus has an important impact on the ductility. When it increases, the covalent nature of the material increases. Direct calculation of Young's modulus from the bulk and shear moduli is avoided in the simulation due to

the existence of many different alternative ways of calculation. Here the Young's modulus is calculated from compliance matrix directly, as it is not influenced by any conventions. Thus it is given as

$$Y_i = \frac{1}{S_i}, \quad i = (x, y, z), \tag{12}$$

where S_i is the inverse of the elastic constants matrix which is also known as the elastic compliance matrix. The calculated Young's modulus is presented in Table 2. The Poisson's ratio on the other hand is indicative of the degree of directionality of the covalent bonds. For covalent materials, the Poisson's ratio is small ($\upsilon = 0.1$), whereas for ionic materials, a typical value of υ is 0.25.[46,47] The interatomic bonding forces can be known from Poisson's ratio. For a brittle material, the Poisson's ratio is very small, whereas for a ductile material, it is larger than 0.33.[48] Poisson's ratio (υ) can be expressed as[49]

$$\upsilon = \frac{1}{2}\left[\frac{B-(2/3)G}{B+(1/3)G}\right]. \tag{13}$$

For fluorite type TiO_2, υ is 0.393, which means that the material is ductile and fluorite has better interatomic bonding forces. Whereas for pyrite-type TiO_2, υ is 0.335. So it can be seen that the pyrite material is also ductile but there exists a weak interatomic bonding force compared to fluorite-type TiO_2. All the calculated values are given in Table 2. For proving the ductility of the crystal, Pugh provided a parameter B/G. If $B/G > 1.75$, then the material is ductile else brittle. For fluorite TiO_2, B/G is 4.34, whereas for pyrite TiO_2, it is 2.71. Both the crystal phases satisfy the Pugh's criteria,[50] both can be treated as a ductile material.

Many high symmetry crystals exhibit a low degree of elastic anisotropy and vice versa.[51] The anisotropy is dependent on the orientation of the elastic modulus. Anisotropic behavior is an important indicator in solid state physics. As such, the zener anisotropic factor is defined as[52]

$$A = \frac{2C_{44}}{(C_{11}-C_{12})}. \tag{14}$$

If any crystal has an anisotropic value of unity, then that material exhibits isotropic properties; whereas if the value is less or more than unity, then it represents a varying degree of anisotropy. Fluorite-type TiO_2 has high symmetry points, so it provides a very low anisotropy of 0.19. However, due to the low symmetry nature of pyrite type TiO_2, it provides a high anisotropy of 0.73. Another way of measurement of elastic anisotropy is the percentage of anisotropy in compression and shear[44,45,52,53]

$$A_{\text{comp}} = \frac{B_{\text{V}} - B_{\text{R}}}{B_{\text{V}} + B_{\text{R}}} \times 100\%, \tag{15}$$

$$A_{\text{shear}} = \frac{G_{\text{V}} - G_{\text{R}}}{G_{\text{V}} + G_{\text{R}}} \times 100\%. \tag{16}$$

For any crystals, these two values can range from 0 (isotropic) to 100% (anisotropy). Here, for the two types of titanium dioxide, the compression anisotropy is very small whereas the shear anisotropy is large.

Again, testing of hardness of the material can be done for polycrystalline material based on the squared Pugh's modulus ratio ($k = G/B$) and the shear modulus (G) as[54]

$$H_{\text{v}} = 2\left(k^2 G\right)^{0.585} - 3. \tag{17}$$

From the calculated Vickers hardness, it can be seen that pyrite-structured TiO_2 is harder than fluorite-structured TiO_2.

3.3. Electronic properties

To illustrate the electronic properties, we focus primarily on two major parameters, namely, the band structure and the total density of state (TDOS). The band structure usually gives a detailed idea about the electronic and optical properties. The energy band structures of cubic fluorite and pyrite single crystals have been calculated along the high symmetry directions in the first Brillouin zone using OLCAO–Perdew–Zunger (PZ) method. The band structures of both crystals are calculated along the special lines connecting the high-symmetry points, $\Gamma(0,0,0)$, $X(1/2,0,0)$, $M(1/2,1/2,0)$, $\Gamma(0.005,0.005,0)$, $R(1/2,1/2,1/2)$ in the k-space.

The energy band diagrams calculated using LDA for both fluorite TiO_2 and pyrite TiO_2 are shown in Fig. 3. It can be seen from Fig. 3 that the Fermi level lies at the lower edge of the conduction band in the fluorite-structured TiO_2 and has a direct band gap with a simulated value of band-gap energy of 0.89 eV, which are the characteristics of a narrow band semiconductor material. It means that the fluorite-structured TiO_2 can absorb light with longer wavelength, which is mainly applied to split water into oxygen and hydrogen. The top of the valence band (valence band maximum, VBM) and the bottom of the conduction band (conduction band minimum, CBM) lie near to the Γ point of the optimized maximum peak of the crystal. The estimated band gap energy is found to be very close to that in Ref. [12], while compared with some other work,[9] the result is contradictory too. As seen from Figs. 3 and 5(a), the electronic structure of fluorite type TiO_2 is mainly influenced by Ti 3d and O 2p states, as the edges of O 2s states are far below the Fermi level, nearly at an edge distance of 8 eV. From Fig. 5(a), it is observed that the unoccupied regions (0.5 eV to 1.5 eV and 2.5 eV to 5 eV) are positioned mainly by Ti 3d states. There are 14 bands which are below the Fermi level and have a width of approximately 8.5 eV. This is primarily due to O 2p states, but has a notable Ti 3d contribution. If compared with other phases of TiO_2, it can be seen that the TDOS of fluorite TiO_2 has some divergent characteristic (which may be due to alternation of the local symmetry throughout the Ti atoms). Except for the splitting

of Ti 3d states (of the empty orbitals), the remaining occupied states between O 2p and Ti 3d (from −8 eV to 0 eV) are however hybridized, which of course provides outcomes, more degree of co-valent bonding between Ti–O of fluorite TiO_2. The major peaks appear on the top of the valence band and the bottom of the conduction band of fluorite-structured TiO_2 near to −5.5 eV, −2.5 eV, 1.5 eV, 2.5 eV, 4 eV, and 4.9 eV respectively, which are due to hybridization of Ti 3d and O 2p orbitals.

The bandgaps given in Refs. [9] and [29] are indirect in nature and found to be 1.061 eV and 1.16 eV, respectively. From the simulation, the band gap found for fluorite TiO_2 varies from 0.89 eV to 1.79 eV. The energy band gap found in this study is ∼ 20% less than DFT-GGA-based simulation[29] and ∼ 16% less than that in Ref. [12]. LDA mostly provides the direct band gap, whereas GGA provides an indirect band gap in most of the simulation studies.[9,12,29] Thus it can be inferred that the simulated energy band gap in this study is quite close to other established approaches.

The simulated energy band diagram for pyrite-type TiO_2 is shown in Fig. 4. It can be seen from the figure that the energy band gap has quite similar behavior to fluorite-type TiO_2 and exhibits an indirect band gap with an energy of 1.18 eV. The VBM lies near to the Γ point and the CBM lies very close to the R point of BZ. As seen from Figs. 4 and 5(b), the electronic structure of pyrite-type TiO_2 is mainly influenced by Ti 3d and O 2p states, as the edges of O 2s states are far below the Fermi level nearly at an edge distance of 9.5 eV. From Fig. 5(b) of total DOS, it is observed that the unoccupied regions (0.5 eV to 3 eV and 4 eV to 6.25 eV) are positioned primarily by Ti 3d states. There are 16 bands which are below the Fermi level and have a width of approximately 6.75 eV. They are primarily due to O 2p states, but have a notable Ti 3d contribution. If compared with other phases of TiO_2, it is seen that the TDOS of pyrite TiO_2 has some divergent characteristic, which is probably due to alternation of the local symmetry throughout the Ti atoms. Except for this splitting of Ti 3d states in empty orbitals, the remaining occupied states between O 2p and Ti 3d (from −6.7 eV to 0 eV) are however hybridized, which means more degree of covalent bonding between Ti–O of pyrite TiO_2. The major peaks appear in the VBM and CBM of pyrite-structured TiO_2 nearly at −5.8 eV, −5.25 eV, 1.8 eV, 2.9 eV, 4.85 eV, and 5.9 eV respectively, which are generated by hybridization of Ti 3d and O 2p orbitals. According to Refs. [9], [12], and [29], the indirect band gap varies from 1.438 eV to 1.451 eV. Here, the simulated band gap is 17.94%–20.27% lower than other simulated results. This is an inherent drawback of DFT and associated difference in crystal structure.

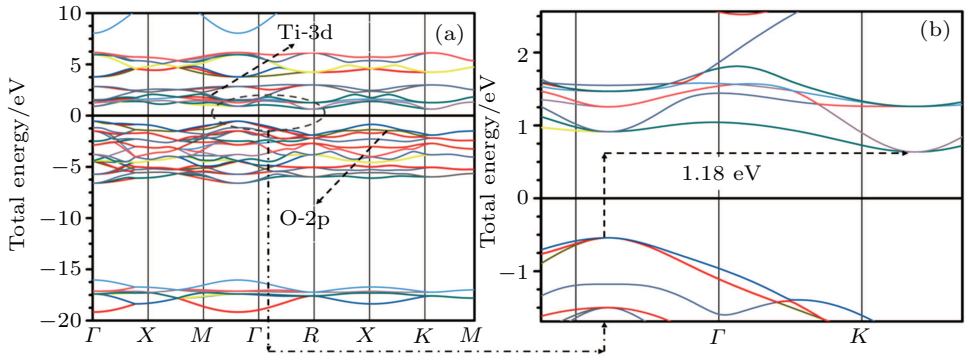


Fig. 4. (color online) (a) Band diagram for pyrite TiO_2 and (b) energy band gap between VBM and CBM.

Another most important material property is the DOS, which also describes the electronic property of a material. In general, it shows the energy representation for describing molecular dynamics and spectroscopy. Mathematically, it is expressed as $g(E)$ which describes the number of quantum states available within an energy range from E to $E + \mathrm{d}E$. In other words, the DOS is a measure of number of electron (or hole) states per unit volume at a given energy. The total densities of state of fluorite TiO_2 and pyrite TiO_2 are illustrated in Figs. 5(a) and 5(b). From Fig. 5, it can be seen that the lowest valence band occurs at −20 eV for fluorite TiO_2 whereas for pyrite TiO_2, it starts well before −20 eV. The valence band between −20 eV and −15 eV in fluorite TiO_2 is mainly contributed by O-s state, whereas in the energy range between −7.5 eV and 0 eV, it is mainly contributed by O-p state. For pyrite TiO_2, the valence band between −20 eV and −13 eV is mainly contributed by O-s state, whereas from −10 eV to 0 eV, it is contributed by O-p state. The highest occupied valence bands for fluorite are essentially dominated by O-1s and Ti-2p states. The Ti-1s state also contributes to the valence band but the density of this state is very small compared to O-1s and Ti-2p states. In the case of pyrite, the highest occupied valence bands are dominated by O-1s and Ti-1s states. A little contribution is also seen from Ti-2p and Ti-3d orbitals towards valence band formation. The lowest occupied conduction band just above the Fermi energy level is mainly contributed by Ti-

3d and O-2p states for both crystals. Other orbital atoms also contribute, but their contributions are negligibly small compared to Ti-3d and O-2p orbital atoms.

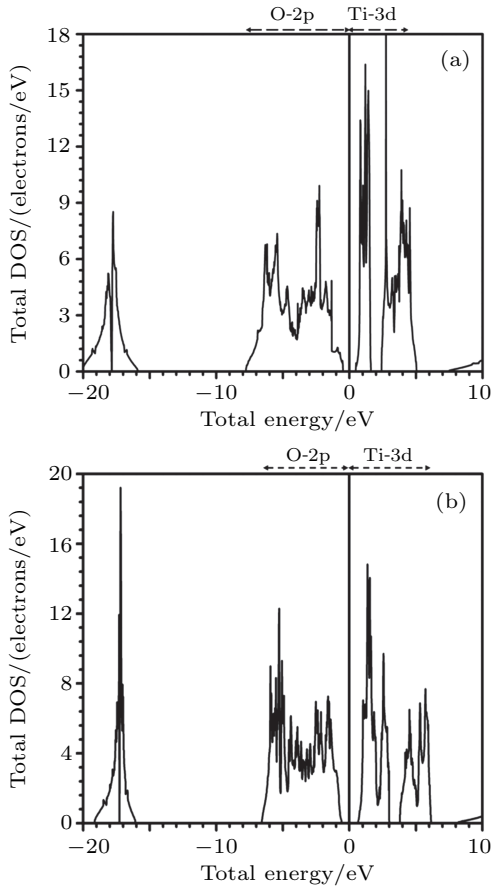


Fig. 5. Total density of states for (a) fluorite TiO_2 and (b) pyrite TiO_2.

4. Conclusion

A simulation-based study is presented here on the structural, mechanical, and electronic properties of high pressurized fluorite and pyrite TiO_2 using orthogonal LCAO basis sets under the framework of DFT. All the results are compared with the previously calculated LDA ones and found an improvement over the elastic properties such as bulk modulus, shear modulus, Young's modulus, Poisson's ratio, and so on. Ductility of both structures of TiO_2 is addressed from their calculated values. It is ensured that all types of ductility conditions are satisfied in both structures of cubic TiO_2. Further, the compound is found to be mechanically stable, elastically anisotropic (tested through various ways) and exhibits ductile property. As there is no perfect experimental data available so far, this work can be considered as very accurate and very much close to work carried out in Refs. [8]–[10], [12], [13], and [21]. The calculated bulk moduli are also very accurate and may be useful for the future study. The calculated lattice parameters of this binary compound are in good agreement with the experimental data with a deviation of less than 1%. Moreover, the band structure with LDA is found to be very much closer to the experimental value. But an underestimated energy bandgap is obtained because a single exchange–correlation potential is not continuous across the gap. The gap can be enhanced in two ways. The first one is to implement Green's function instead of density functional theory. The Green's function can help to study self-energy of quasi particles in a many-particle system. The second way can be applying self-interaction correction (SIC). Here, self-interaction in the Hartree term is removed by an orbital-by-orbital correction to the exchange–correlation potential. The detailed investigation on DOS is carried out to understand the fluorite and pyrite TiO_2 structures.

References

[1] J Z Zhao, G T Wang and Y C Liang 2008 *Chin. Phys. Lett.* **25** 4356
[2] Landmann M, Rauls E and Schmidt W G 2012 *J. Phys.: Condens. Matter* **24** 1
[3] Fan L B, Zhang P, Has S, Wang Y X, Liu P D, Wang W and Yao Y G 2007 *Physics* 36
[4] Xie H, Hou W and Bai W 2005 *Physics* **34**
[5] Wang J H, Li Z P, Liu B and Liu B B 2017 *Chin. Phys. B* **26** 026101
[6] Wang X, Shi Z and Jiang J 2009 *Physics* **38**
[7] Wan L, Cao L, Zhang W H, Han Y Y, Chen T X, Liu L Y, Guo P P, Feng J Y and Xu F Q 2012 *Acta Phys. Sin.* **61** 186801 (in Chinese)
[8] Miloua R, Kebbab Z, Benramdane N, Khadraoui M and Chiker F 2011 *Computational Material Science* **50** 2142
[9] Jun L Q, Zhang N C, Liu F S and Liu Z T 2014 *Phys. Scr.* **89** 1
[10] Zhou X F, Dong X, Qian G R, Zhang L, Tian Y and Wang H T 2010 *Phys. Rev. B* **82** 1
[11] Zhang J, Zhou P, Liu J and Yu J 2014 *Phys. Chem. Chem. Phys.* **16** 20382
[12] Mahmood T, Cao C, Tahir M, Idrees F, Ahmed M, Tanveer M, Aslam I, Usman Z, Ali Z and Hussain S 2013 *Physica B* **420** 74
[13] Liang Y, Zhang B and Zhao J 2008 *Phys. Rev. B* **77** 1
[14] Kong X G, Yu Y and Gao T 2010 *Eur. Phys. J. B.* **76** 365
[15] Swamy V and Muddle B C 2007 *Phys. Rev. Lett.* **98** 035502
[16] Mattesini M, Almeida J S de, Dubrovinsky L, Dubrovinskaia N, Johansson B and Ahuja R 2004 *Phys. Rev. B* **70** 115101
[17] Mattesini M, Almeida J S de, Dubrovinsky L, Dubrovinskaia N, Johansson B and Ahuja R 2004 *Phys. Rev. B* **70** 212101
[18] Kim D Y, Almeida J S de, Koci L and Ahuja R 2007 *Appl. Phys. Lett.* **90** 171903
[19] Wang Y Y, Ding J H, Liu W B, Huang S S, Ke X Q, Wang Y Z, Zhang C and Zhao J J 2017 *Chin. Phys. B* **26** 026102
[20] Hu X L, Zhao R X, Luo Y and Song Q G 2017 *Chin. Phys. B* **26** 023101
[21] Muscat J, Swamy V and Harrison N M 2002 *Phys. Rev. B* **65** 224112
[22] Broyden C G 1970 *J. Inst. Maths Applics* **6** 76
[23] Fletcher R 1970 *Computer Journal* **13** 317
[24] Goldfarb D 1970 *Mathematics of Computation* **24** 23
[25] Shanno D F 1970 *Mathematics of Computation* **24** 657
[26] Ching W Y, Xu Y N and French R H 1996 *Phys. Rev. B* **54** 13546
[27] Perdew J P and Zunger A 1981 *Phys. Rev. B* **23** 5048
[28] Monkhorst H J and Pack J D 1976 *Phys. Rev. B* **13** 5188
[29] Zhu T and Gao S P 2014 *J. Phys. Chem. C* **118** 11385
[30] Atomistix ToolKit version 2014.3, QuantumWise A/S (www.quantumwise.com)
[31] Brandbyge M, Mozos J L, Ordejón P, Taylor J and Stokbro K 2002 *Phys. Rev. B* **65** 165401
[32] Soler J M, Artacho E, Gale J D, García A, Junquera J, Ordejón P and Sánchez-Portal D 2002 *J. Phys.: Condens. Matter* **14** 2745
[33] Birch F 1947 *Phys. Rev. B* **71** 809
[34] Murnaghan F D 1944 *Proc. Natl. Acad. Sci. USA* **30** 244
[35] Lu W, Wang H, Hu Y, Huang H and Gu H 2009 *Physica B* **404** 79
[36] Delogoz E, Ozisik H, Colakoglu K, Surucu G and Ciftci Y O 2011 *J. Alloy Compd.* **509** 1711

[37] Ozisik H, Deligoz E, Colakoglu K and Ciftci Y O 2011 *Com. Mat. Sci.* **50** 1057
[38] Ozisik H, Deligoz E, Colakoglu K and Surucu G 2010 *Phys. Status Solidi* **4** 347
[39] Ateser E, Ozisik H, Colakoglu K and Deligoz E 2011 *Com. Mat. Sci.* **50** 3208
[40] Born M and Huang K 1982 *Dynamical Theory and Experiment* Springer, Vol. 1
[41] Wu Z J, Zhao E J, Xiang H P, Hao X F, Liu X J and Meng J 2007 *Phys. Rev. B* **76** 1
[42] Reuss Von A 1929 *Z. Angew Math. Mech.* **9** 149
[43] Voight W 1928 *Lehrbuch der Kristallphysik: Verlag und Druck, Von B. G. Teubner in Leipzig und Berlin* **9** 62
[44] Hill R 1952 *Proc. Phys. Soc.* **65** 349
[45] Simmons G and Wang H 1971 *Single Crystal Elastic Constants and Calculated Aggregate Properties: A Handbook*, (Cambridge: MIT Press)
[46] Bannikov V V, Shein I R and Ivanovskii A L 2007 *Phys. Stat. Sol.* **3** 89
[47] Fu H, Li D, Peng F, Gao T and Cheng X 2008 *Comp. Mat. Sci.* **44** 774
[48] Clark Stewart J, Segall Matthew D, Pickard Chris J, Hasnip Phil J, Probert Matt I J, Refson K and Payne M C 2005 *Z. Kristallogr* **220** 567
[49] Caravaca M A, Mino J C, Perez V J, Casali R A and Ponce C A 2009 *J. Phys.: Condens. Matter* **21** 1
[50] Pugh S F 1954 *The London, Edinburgh, and Dublin Philosophical Magazine and Journal of Science* **45** 823
[51] Tvergaard V and Hutchinson J W 1988 *J. Am. Chem. Soc.* **71** 157
[52] Tripathy S K and Kumar V 2014 *Material Science and Engineering B* **182** 52
[53] Chung D H, Buessem W R, Vahldiek F W and Mersol S A 1968 (New York: Plenum Press)
[54] Chen X Q, Niu H, Li D and Li Y 2011 *Intermettalics* **19** 1275